

**UNCLASSIFIED**



**Australian Government**

**Department of Defence**

Science and Technology

# **Finite Element Modelling of Heat Exchange with Thermal Radiation**

*Leonid K Antanovskii*

**Weapons and Combat Systems Division**

Defence Science and Technology Group

DST-Group-TR-3345

## **ABSTRACT**

This report addresses the mathematical and numerical modelling of heat exchange in a solid object with the effect of thermal radiation included. Three models are analysed, the general three dimensional model and two approximate models. Based on Finite Element Method (FEM), a fully vectorized MATLAB<sup>®</sup> solver is developed for the three models, and simulation results are compared. The developed code can be used to enhance the VIRSuite software developed in DST Group for simulation of weapon-target engagement.

**RELEASE LIMITATION**

*Approved for public release*

**UNCLASSIFIED**

UNCLASSIFIED

*Published by*

*Weapons and Combat Systems Division  
Defence Science and Technology Group  
PO Box 1500  
Edinburgh, South Australia 5111, Australia*

*Telephone: 1300 333 362  
Facsimile: (08) 7389 6567*

*© Commonwealth of Australia 2017  
February, 2017  
AR-016-809*

**APPROVED FOR PUBLIC RELEASE**

UNCLASSIFIED

# Finite Element Modelling of Heat Exchange with Thermal Radiation

## Executive Summary

This report addresses the mathematical and numerical modelling of heat exchange in a solid object with the effect of thermal radiation included. Three models are analysed, the general three dimensional model and two approximate models. Based on Finite Element Method (FEM), a fully vectorized MATLAB<sup>®</sup> solver is developed for the three models, and simulation results are compared. The developed code can be used to enhance the VIRSuite software developed in DST Group for simulation of weapon-target engagement.

It is recommended to seriously consider an option to employ hybrid meshes, which will be composed of 1D, 2D and 3D finite elements linked together with specially designed transition elements. A particular target can be better approximated by such elements, opening an opportunity for real-time simulation of very complex targets.

UNCLASSIFIED

THIS PAGE IS INTENTIONALLY BLANK

UNCLASSIFIED

## Author

### **Leonid K Antanovskii**

Weapons and Combat Systems Division

Born in Siberia, Leonid Antanovskii holds a Master of Science (with distinction) in Mechanics and Applied Mathematics from the Novosibirsk State University and a PhD in Mechanics of Fluid, Gas and Plasma from the Lavrentyev Institute of Hydrodynamics of the Russian Academy of Science. Since graduation he worked for the Lavrentyev Institute of Hydrodynamics (Russia), Microgravity Advanced Research & Support Center (Italy), the University of the West Indies (Trinidad & Tobago), and in private industry in the USA and Australia.

Leonid Antanovskii joined the Defence Science and Technology Group in February 2007 working in the area of weapon-target interaction.

---

UNCLASSIFIED

THIS PAGE IS INTENTIONALLY BLANK

UNCLASSIFIED

## Contents

1	INTRODUCTION . . . . .	1
2	PROBLEM FORMULATION . . . . .	2
3	APPROXIMATE MODELS . . . . .	3
4	NUMERICAL SCHEME . . . . .	4
5	SIMULATION RESULTS . . . . .	6
6	DISCUSSION . . . . .	8
7	REFERENCES . . . . .	8
	APPENDIX A: FIGURES . . . . .	9

## List of Figures

A1	Temperature distribution on a 10 mm-thick block surface (1D results) . . . . .	9
A2	Temperature distribution on a 10 mm-thick block surface (2D results) . . . . .	9
A3	Temperature distribution on a 10 mm-thick block surface (3D results) . . . . .	10
A4	Temperature distribution on a 100 mm-thick block surface (1D results) . . . . .	10
A5	Temperature distribution on a 100 mm-thick block surface (2D results) . . . . .	11
A6	Temperature distribution on a 100 mm-thick block surface (3D results) . . . . .	11
A7	Temperature distribution on Wall2 (1D results) . . . . .	12
A8	Temperature distribution on Wall2 (2D results) . . . . .	12
A9	Temperature distribution on Wall2 (3D results) . . . . .	13
A10	Temperature distribution on Wall3 (1D results) . . . . .	13
A11	Temperature distribution on Wall3 (2D results) . . . . .	14
A12	Temperature distribution on Wall3 (3D results) . . . . .	14
A13	Engine block model . . . . .	15
A14	Temperature distribution near engine block (1D results) . . . . .	15
A15	Temperature distribution near engine block (2D results) . . . . .	16
A16	Temperature distribution near engine block (3D results) . . . . .	16

UNCLASSIFIED

THIS PAGE IS INTENTIONALLY BLANK

UNCLASSIFIED

# 1 Introduction

For real-time simulation of an engagement of a missile equipped with an infra-red sensor and a target radiating thermal heat, it is important to develop a numerical model for the sensor *seeing* a particular object dynamically. This means that, due to the motion of the weapon and potentially of the target, the sensor detects the target from different view points, and therefore the thermal radiation will be different. Because of this relative motion, some surface patches of the target may be in shadow, being obscured by other objects. For real-time simulations, the calculation of the view factors is the most time-consuming procedure [Siegel & Howell 2002, Modest 2003, Jacobs 2006].

At the same time we need to know the temperature distribution along the target surface in order to calculate thermal radiation governed by the Stefan-Boltzmann law. Since a target engagement has a relatively short duration as compared to the characteristic time of temperature change, the transient distribution of temperature can be pre-calculated before the real-time simulations are conducted. In rare circumstances, when the target is manoeuvring at a high speed and acceleration to avoid the weapon hit, the temperature field may change due to the aerodynamic heating even during the short time of engagement. This situation is obviously more complicated as the problem of computation of the temperature field becomes coupled with the target motion.

The VIRSuite software developed in DST Group is designed to provide real-time simulation of weapon-target interaction. The underlying data structure is based on a triangular mesh representing the target skin, each facet of which has given thickness and material properties. The temperature field changes across the facet thickness in real time. No heat conduction along the surface is taken into account. This data structure is suitable for the calculation of surface radiation but has known deficiency when approximating models which do not have thin surface layers.

We propose to use different data structures for different types of simulation, namely, the triangular mesh for real-time simulation used by VIRSuite, and a 3D mesh for high-fidelity simulation. The 3D element should be either a tetrahedron or a triangular prism to be compatible with the boundary mesh composed of triangular facets. The pre-calculated temperature distribution over the boundary can be used as an input into the VIRSuite software which does not need to compute heat flow across the target skin any more, and therefore will be even better performing.

The effect of 3D diffusion on thermal radiation is demonstrated in [Swierkowski et al. 2014]. It is shown the expected superiority of the 3D model for calculating heat diffusion around a chunky section of a target, such as an engine room.

In this report the mathematical and numerical models for heat transfer are described. A code prototype is developed in MATLAB. For comparison different approximations with VIRSuite data structure, a utility translating the VIRSuite triangular mesh equipped with thickness to a 3D mesh composed of triangular prisms is also developed. A copy of the code may be released on request.

## 2 Problem formulation

The mathematical model for heat flow in and around a target must take into account various physical effects, ranging from conduction and convection to thermal radiation. In fact this is a coupled problem to be solved simultaneously with the ambient atmosphere. The full system of continuum mechanics equations has to be solved in the general case, because the density, velocity, pressure and temperature fields are coupled. In a simplified situation the effect of atmosphere can be modelled by boundary conditions, and therefore the temperature field needs to be computed inside the target only.

Let  $\mathcal{D}$  be a domain occupied by a solid body in the three-dimensional space. Assuming the solid body to be non-deformable, we choose a coordinate system co-moving with the rigid body. Let  $\vec{x}$  be the position vector,  $t$  the time, and denote the boundary of the solid body by  $\partial\mathcal{D}$ . Our task is to find the temperature field  $T = T(\vec{x}, t)$  as the solution to the heat conductivity equation

$$\rho c_p \frac{\partial T}{\partial t} - \nabla \cdot (\kappa \nabla T) = Q \quad \text{in } \mathcal{D}, \quad (1)$$

with the boundary condition

$$-\vec{n} \cdot (\kappa \nabla T) = q \quad \text{on } \partial\mathcal{D}, \quad (2)$$

and the initial condition

$$T = T_0 \quad \text{at } t = 0. \quad (3)$$

Here  $\rho$  is the mass density,  $c_p$  the specific heat capacity,  $\kappa$  the thermal conductivity,  $Q$  the volume density of heat sources, and  $q$  the heat flux along the inward normal vector  $\vec{n}$  at the boundary  $\partial\mathcal{D}$ . The heat source  $Q$  models heat generated inside the target, say, by the target engine, but must set zero otherwise. Note that, according to Fourier's law, the heat flux  $\vec{q}$  is given by the formula

$$\vec{q} = -\kappa \nabla T \quad (4)$$

and therefore the boundary condition states  $\vec{q} \cdot \vec{n} = q$ . Since the normal vector  $\vec{n}$  is inward, the normal flux  $q$  represents heat flowing into the domain  $\mathcal{D}$ .

In the general case the material properties  $\rho$ ,  $c_p$  and  $\kappa$ , and the right-hand sides  $Q$  and  $q$  are given functions of temperature. For example, the Stefan-Boltzmann thermal radiation law specifies the normal component of the heat flux

$$q^{\text{SB}}(T) = \sigma \varepsilon(T) T^4 \quad (5)$$

where  $\sigma$  is the Stefan-Boltzmann constant and  $\varepsilon$  the emissivity coefficient which generally depends on the absolute temperature  $T$ . The Stefan-Boltzmann heat flux must contribute to  $q$  with the minus sign because it describes the outgoing energy. Adsorption of incoming energy by the surface  $\partial\mathcal{D}$  is modelled by additional physical parameters. For example, the adsorption of solar radiation is specified by solar intensity  $I$  and solar adsorptivity coefficient  $\alpha$ . It is worthwhile emphasizing that infra-red sensors detect a portion of the total flux  $q^{\text{SB}}(T)$  corresponding to a particular bandwidth.

### 3 Approximate models

Let us assume that the domain  $\mathcal{D}$  is thin in one direction, and thus can be represented by a surface  $\mathcal{S}$  equipped with thickness  $h$  and a unit normal vector  $\vec{n}$ . In other words, the domain  $\mathcal{D}$  is parametrized by the mapping

$$\mathcal{S} \times \mathbb{R} \ni (\vec{x}, z) \mapsto \vec{x} + z \vec{n}(\vec{x}) \in \mathcal{D}. \quad (6)$$

This parametrization is invertible in the layer  $0 \leq z \leq h(\vec{x})$  provided that the surface  $\mathcal{S}$  is smooth and  $h$  is small enough compared to the principal radii of the surface curvature.

We call the surface  $\mathcal{S}$  the outer boundary of  $\mathcal{D}$ , corresponding to  $z = 0$ , and the surface  $z = h(\vec{x})$  the inner boundary. We get the decomposition

$$\nabla = \nabla_{\mathcal{S}} + \vec{n} \frac{\partial}{\partial z} \quad (7)$$

where  $\nabla_{\mathcal{S}}$  is the surface gradient. The normal vector  $\vec{n}$  is inward with respect to  $\mathcal{D}$  at the outer boundary  $\mathcal{S}$ , and is close to the outward normal vector at the inner boundary if the surface gradient of the thickness,  $\nabla_{\mathcal{S}} h$ , is negligible with respect to the unity.

Let us now assume that heat predominantly flows across the thickness, so the heat flux  $\vec{q}$  is nearly orthogonal to the surface  $\mathcal{S}$ . This is equivalent to the statement that

$$|\nabla_{\mathcal{S}} T| \ll \left| \frac{\partial T}{\partial z} \right|, \quad (8)$$

and hence the governing equations reduce to the following problem

$$\rho c_p \frac{\partial T}{\partial t} = \frac{\partial}{\partial z} \left( \kappa \frac{\partial T}{\partial z} \right) + Q \quad \text{for } 0 < z < h(\vec{x}), \quad (9)$$

$$-\kappa \frac{\partial T}{\partial z} = q^0 \quad \text{at } z = 0, \quad \kappa \frac{\partial T}{\partial z} = q^h \quad \text{at } z = h(\vec{x}), \quad (10)$$

where  $q^0$  and  $q^h$  are the heat fluxes through the outer and inner boundaries, respectively. Note that the point  $\vec{x}$  of the surface  $\mathcal{S}$  is just a parameter in this formulation.

If  $h$ ,  $\rho$ ,  $c_p$  and  $\kappa$  are approximated by constants at each facet, one needs to solve a series of heat conductivity equations per facet. These equations are independent and therefore can be solved simultaneously in separate threads. This one-dimensional model is implemented in VIRSuite.

The reduced system of equations can be formally obtained by scaling  $h$  (and  $z$  respectively) by a small factor  $\epsilon$ ,  $\kappa$  by  $\epsilon^2$  that demands scaling  $q$  by  $\epsilon$ , and then retaining only the leading-order terms in the governing equations. In a dimensionless form, this formal procedure corresponds to the following asymptotic conditions

$$h \ll \Delta x, \quad \frac{\rho c_p}{\Delta t} \approx \frac{\kappa}{h^2} \gg \frac{\kappa}{\Delta x^2}, \quad (11)$$

where  $\Delta x$  is the characteristic length scale along the surface, and  $\Delta t$  is the characteristic time scale.

For example, let us choose  $h \approx 0.04$  m which is negligible compared to the typical size of a target, say  $\Delta x \approx 4$  m. For Steel (1% Carbon) with material properties

$$\rho = 7800 \frac{\text{kg}}{\text{m}^3}, \quad c_p = 473 \frac{\text{J}}{\text{kg K}}, \quad \kappa = 43 \frac{\text{W}}{\text{m K}}, \quad (12)$$

we get the condition for the characteristic time scale  $\Delta t \approx 137$  s. For Aluminum with material properties

$$\rho = 2770 \frac{\text{kg}}{\text{m}^3}, \quad c_p = 884 \frac{\text{J}}{\text{kg K}}, \quad \kappa = 201 \frac{\text{W}}{\text{m K}}, \quad (13)$$

we get somewhat smaller value of  $\Delta t \approx 19$  s. The latter poses a restriction on the rate of change of heat fluxes in time. Note that  $\Delta t$  can be thought of as the characteristic time of propagation of a heat wave.

Let us now analyse the opposite situation when heat flows predominantly along the target skin. This is equivalent to the statement that

$$|\nabla_S T| \gg \left| \frac{\partial T}{\partial z} \right|. \quad (14)$$

Such a situation arises when the inner surface of the skin is well insulated. In this case temperature is nearly uniform across thickness, and the reduced governing equations are obtained by averaging the general equation (1) in the normal direction. As a result we obtain the following equation

$$\rho c_p h \frac{\partial T}{\partial t} - \nabla_S \cdot (\kappa h \nabla_S T) = Q h + q^0 + q^h \quad \text{on } \mathcal{S}. \quad (15)$$

Notice the thickness  $h$  appearing as a factor in the equation coefficients.

It is natural to associate the governing equations (1), (15) and (9) with the 3D, 2D and 1D problems, respectively. This association corresponds to the number of independent spatial variables. The choice of either 1D or 2D model must be dictated by the asymptotic conditions (8) and (14), respectively. The 3D model is free of any assumption as, in fact, does not contain the concept of surface thickness.

## 4 Numerical scheme

Finite Element Method (FEM) is well suited for solution of heat exchange problems. We approximate the absolute temperature  $T$  in the 3D problem (1)–(2) by the finite sum

$$T(\vec{x}, t) = \sum_i N_i(\vec{x}) T_i(t) \quad (16)$$

where  $N_i(\vec{x})$  is the shape function associated with a node numbered by  $i$ . Upon substituting this representation into the governing equation, multiplying the result by a weighting function  $W_k(\vec{x})$  and integrating by parts, we get the system of ordinary differential equations

$$\sum_i \left( M_{ki} \frac{dT_i}{dt} + S_{ki} T_i \right) = F_k \quad (17)$$

where

$$M_{ki} = \int_{\mathcal{D}} \rho c_p W_k N_i dV, \quad (18)$$

$$S_{ki} = \int_{\mathcal{D}} \kappa \nabla W_k \cdot \nabla N_i dV, \quad (19)$$

$$F_k = \int_{\mathcal{D}} W_k Q dV + \int_{\partial\mathcal{D}} W_k q dA. \quad (20)$$

Here  $dV$  is the volume element and  $dA$  is the area element. The coefficients  $M_{ki}$  and  $S_{ki}$  are called the mass and stiffness matrix, respectively, and  $F_k$  is called the load vector. Strictly speaking, the system of equations (17) becomes a system of ordinary differential equations when resolved with respect to time derivatives. The latter is achieved by inverting the mass matrix.

It is a common practice to move temperature-dependent terms of  $Q$  and  $q$  from the load vector to the stiffness matrix. For example, if  $Q = \hat{Q} - B(T)T$  and  $q = \hat{q} - \beta(T)T$  then

$$S_{ki} = \int_{\mathcal{D}} \kappa \nabla W_k \cdot \nabla N_i dV + \int_{\mathcal{D}} B W_k N_i dV + \int_{\partial\mathcal{D}} \beta W_k N_i dA, \quad (21)$$

$$F_k = \int_{\mathcal{D}} W_k \hat{Q} dV + \int_{\partial\mathcal{D}} W_k \hat{q} dA. \quad (22)$$

In particular, we get  $\beta = \sigma \varepsilon(T) T^3$  for the Stefan–Boltzmann radiation. The term  $\hat{q}$  describes other heat fluxes such as solar adsorption and aerodynamic heating provided that they do not depend on temperature.

The system of ordinary differential equations (17) can be solved by various numerical schemes, such as a family of Runge–Kutta schemes, some of which are capable of automatically selecting the time step to achieve a desired accuracy. The backward Euler scheme with ‘frozen’ coefficients taken from the previous time level is implemented as follows

$$\sum_i (M_{ki}^o + S_{ki}^o \tau) T_i = \sum_i M_{ki}^o T_i^o + F_k^o \tau \quad (23)$$

where  $\tau$  is the time step, and the superscript ‘naught’ is supplied to quantities evaluated at the previous time level. The numerical scheme is implicit and does not pose severe limitations on the time step  $\tau$ . If the material properties strongly depend on temperature, a few iterations can be conducted to improve accuracy. In this case the solution to the system of equations (23) is called the predictor, and the iterated solution with updated material properties at the current time level is called the corrector.

We have briefly described the Bubnov–Galerkin method [Zienkiewicz & Taylor 1989] which reduces to the Galerkin method when the weighting functions coincide with the shape functions, namely when  $W_k = N_k$ . In this case the mass and stiffness matrices become symmetric. Note that the Bubnov–Galerkin method is indispensable when heat convection is modelled. Since this effect is not accounted for, we use exclusively the Galerkin method in the following numerical simulations.

## 5 Simulation results

In the simulations below the heat source intensity is equal to  $I = 1000 \text{ W/m}^2$ , and the radiation flux direction is given by the expression

$$\vec{d}_s(t) = -(\cos(\pi t/t_0), 0, \sin(\pi t/t_0)) \quad (24)$$

where  $t_0 = 1000 \text{ s}$ . The initial distribution of temperature is  $T_0 = 300 \text{ K}$  which is also the equilibrium temperature of the Stefan–Boltzmann thermal radiation at the outer surface  $\mathcal{S}$ . For the sake of simplicity, we do not calculate view factors but only compute the heat flux according to the direction of the normal vector. The inner surface is insulated. In other words,

$$q^0 = I \alpha \max(\vec{d}_s(t) \cdot \vec{n}, 0) + \sigma \varepsilon (T_0^4 - T^4), \quad q^h = 0. \quad (25)$$

Recall that the unit normal vector  $\vec{n}$  to the outer surface  $\mathcal{S}$  is inward to the body  $\mathcal{D}$ .

The data structure employed by VIRSuite consists of a triangular mesh each facet of which is equipped with thickness. To run 3D simulations, we need to convert the triangular surface mesh to a triangular prism mesh. This is achieved by assigning normal vectors to each node of the surface using the available normal vectors to the facets, and then creating a stack of triangular prisms by adding new nodes along the node-based normals. The index from the triangular prism element to the parent facet has to be calculated to populate the element attributes with material properties taken from the parent facet. This procedure may result in a severely distorted 3D mesh when the surface is not smooth and thickness is not small, for example, when the surface has corners.

First we set up a benchmark model problem. Consider the surface of a block of dimension 10-by-8-by-5 metres, and tessellate it using 250 mm spacing size. The material is Steel with the physical properties (12), and select  $\alpha = 1$  and  $\varepsilon = 1$ . The number of elements across thickness is 10. In the 3D model this is the number of prisms, and in the 1D problem employed by VIRSuite this is the number of elements.

Figures A1–A3 show the final temperature distribution at the block surface for uniform thickness  $h = 10 \text{ mm}$ . As expected, the 1D simulation results provide uniform temperature at all faces of the block because each facet of the face has the same angle with the source direction, and no heat diffusion is taken into account. Unlike the 1D case, the 2D and 3D simulation results show non-uniform temperature distribution. It is seen spurious undershooting and overshooting of temperature in 3D simulations because the triangular prism elements are very thin. Indeed, the ratio of the prism height to the facet size is  $1/250$ . Otherwise, the results match quite accurately.

Figures A4–A6 show the final temperature distribution at the block surface for uniform thickness  $h = 100 \text{ mm}$ . As before, the 1D simulation results provide uniform temperature at all faces of the block but the 2D and 3D simulation results show non-uniform temperature distribution. Spurious undershooting and overshooting of temperature in the 3D simulations was observed due to the thin triangular prism elements; the ratio of the prism height to the facet size is  $1 : 25$ .

Most of the VIRSuite models fail to run after the transformation of the surface mesh to triangular prism mesh. This is because the transformation (6) becomes singular when the

model contains very fine details. All the VIRSuite meshes contain free edges indicating that the models are composed of several separate shapes which apparently do not share nodes. Even a couple of models contain unreferenced nodes which must be removed to make the FEM matrix non-singular.

We have succeeded to simulate only two simple models of VIRSuite in both 2D and 3D cases, which are originally named Wall2 and Wall3. All the material properties including adsorptivity  $\alpha$  and emissivity  $\varepsilon$  are loaded from the VIRSuite database.

The simulation results for Wall2 are shown in Figures A7–A9. It is seen that the 1D and 3D results match each other much better than the 2D results.

The simulation results for Wall3 are shown in Figures A10–A12. Unlike Wall2, all the 1D, 2D and 3D results match each other much better though undershooting and overshooting of temperature is seen in both 2D and 3D simulation results.

The last example demonstrates the expected superiority of the 3D model for calculating heat diffusion when the thermal gradient is not normal to the target surface [Swierkowski et al. 2014]. We considered a plate made of steel (1% Carbon) and of dimensions 4-by-3 metres and of constant thickness  $h = 100$  mm. The plate is a schematic representation of a section of the target wall with an engine block attached to the wall by means of four legs as shown in Figure A13. The engine was kept at a high temperature which diffuses to the outer wall surface. The Stefan–Boltzmann thermal radiation was imposed at the outer surface but the solar radiation was suppressed for simplicity. The inner surface was insulated except for the four rectangular patches which gave a heat flux according to the Biot boundary condition. In this case we had the following boundary conditions

$$q^0 = \sigma \varepsilon (T_0^4 - T^4), \quad q^h = \beta (T_1 - T), \quad (26)$$

where  $T_0$  is the equilibrium temperature of the radiative surrounding,  $T_1$  is the onset engine temperature and  $\beta$  is the heat exchange coefficient. The rectangular patches schematically model the contact areas on the plate from the four legs of the engine. The Biot coefficient  $\beta$  vanishes outside the contact patches.

In the numerical simulation we set  $T_0 = 300$  K,  $T_1 = 500$  K and  $\beta = 1$  kW/m<sup>2</sup>/K. The 1D, 2D and 3D simulations start with the initial temperature  $T_0$  and the physical time duration of the simulated heat diffusion is 1 hour. The computational time depends on the numerical time-step  $\tau$  which in general is much shorter than the physical time, especially for long time-steps.

Figure A14 shows the final distribution of temperature calculated by the 1D model. In the absence of lateral heat diffusion, the resultant temperature field is piecewise constant, reflecting sharp boundaries between surface facets. Figure A15 shows the final distribution of temperature calculated by the 2D model. It demonstrates the opposite extreme case of too extended propagation of heat wave in the lateral directions. As expected, the 3D model results shown in Figure A16 are more realistic. In contrast to the 1D model results, the temperature distribution spreads beyond the areas of contact with the hot engine, attaining quite large values between the contact patches. However, compared to the 2D results, the temperature field is more localized near the engine legs.

The simulation time of the 3D model is significantly greater than that of the 1D and 2D models and it is not feasible to apply the 3D solver for real-time simulation. It has been implemented,

however, in the off-line module for prediction of initial pre-engagement signatures.

## 6 Discussion

A mathematical model for 3D heat transfer and a numerical model based on FEM are described. A code prototype for VIRSuite enhancement was developed in MATLAB.

An issue with the mesh quality was identified. This issue does not manifest itself in VIRSuite because the facet geometry is used for visualization only. However, in both 2D and 3D simulation the mesh quality must be good enough to produce accurate results. In fact, poor surface mesh composed of very distorted facets did not allow the mesh conversion utility to produce non-singular triangular prisms from facets.

Alternatively, one should consider an application of a hybrid mesh, composed of 3D, 2D and even 1D elements linked with specially designed transition elements. In this case a 3D mesh will approximate thick chunks of the target only as there is no need to employ the expensive 3D solver in thin sections, whereas a 2D mesh will approximate thin sections of the target. Finally, 1D elements equipped with cross-section area will approximate target spikes such as antennas and wires.

## 7 References

- Jacobs, P. A. (2006) *Thermal Infrared Characterization of Ground Targets and Backgrounds*, Vol. TT70 of *Tutorial Texts in Optical Engineering*, SPIE Press, Bellingham, Washington.
- Modest, M. F. (2003) *Radiative Heat Transfer*, 2nd edn, Academic Press, Amsterdam.
- Siegel, R. & Howell, J. R. (2002) *Thermal Radiation Heat Transfer*, 4th edn, Taylor & Francis, New York.
- Swierkowski, L., Christie, C. L., Antanovskii, L. K. & Gouthas, E. (2014) Real-time scene and signature generation for ladar and imaging sensors, in *SPIE Defense and Security 2014 Symposium*, Baltimore, USA.
- Zienkiewicz, O. C. & Taylor, R. L. (1989) *The Finite Element Method*, Vol. 1: Basic Formulation and Linear Problems, 4th edn, McGraw-Hill, London.

## Appendix A: Figures

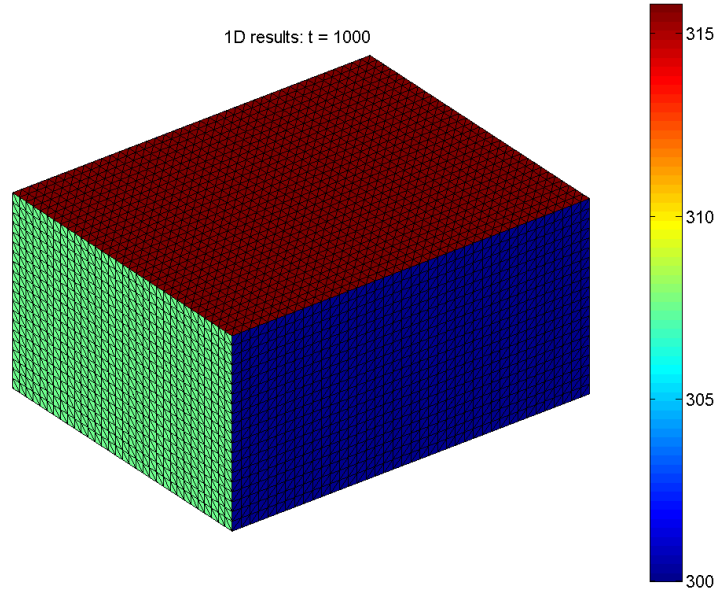


Figure A1: Temperature distribution on a 10 mm-thick block surface (1D results)

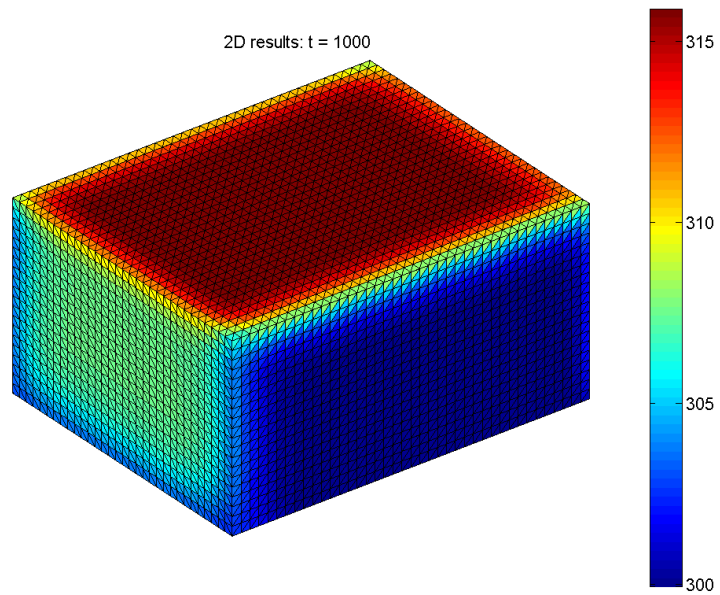


Figure A2: Temperature distribution on a 10 mm-thick block surface (2D results)

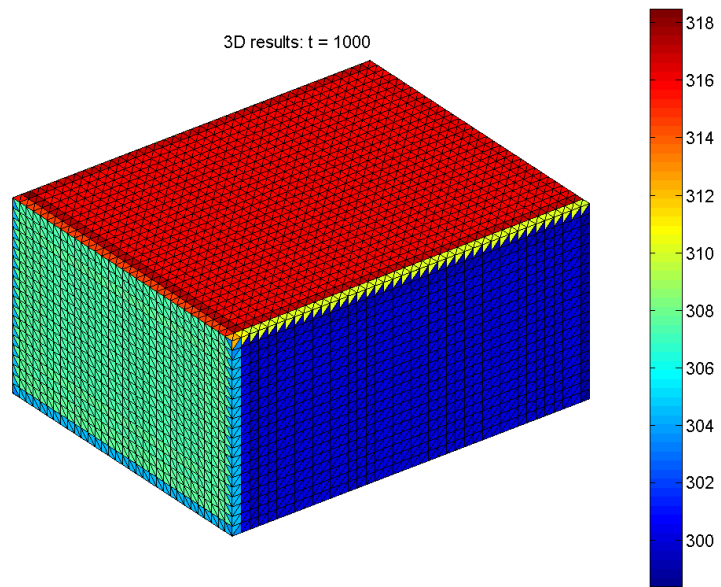


Figure A3: Temperature distribution on a 10 mm-thick block surface (3D results)

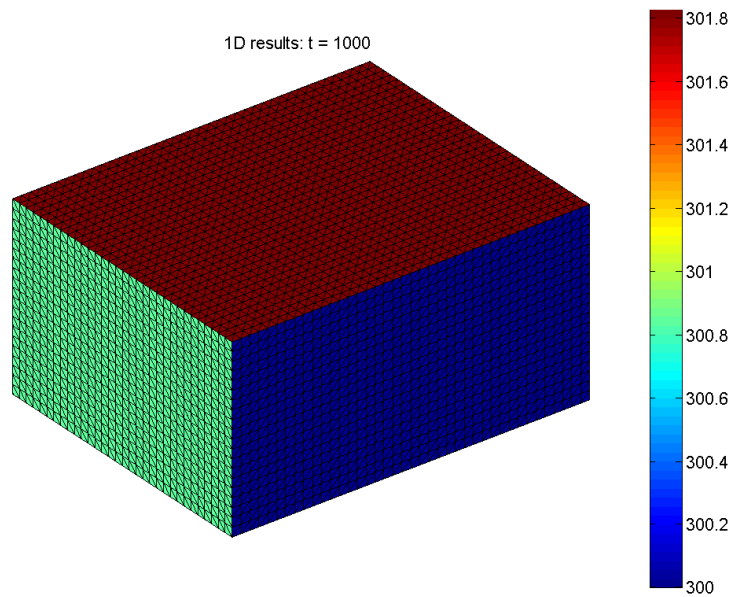


Figure A4: Temperature distribution on a 100 mm-thick block surface (1D results)

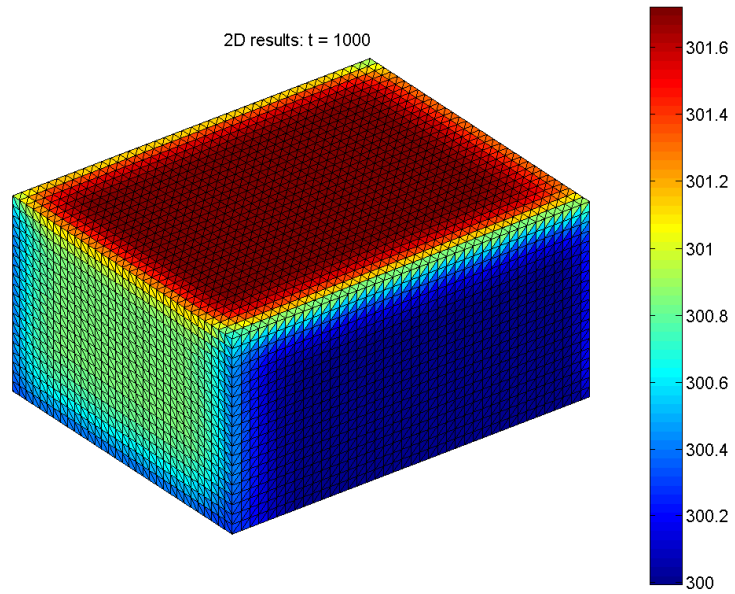


Figure A5: Temperature distribution on a 100 mm-thick block surface (2D results)

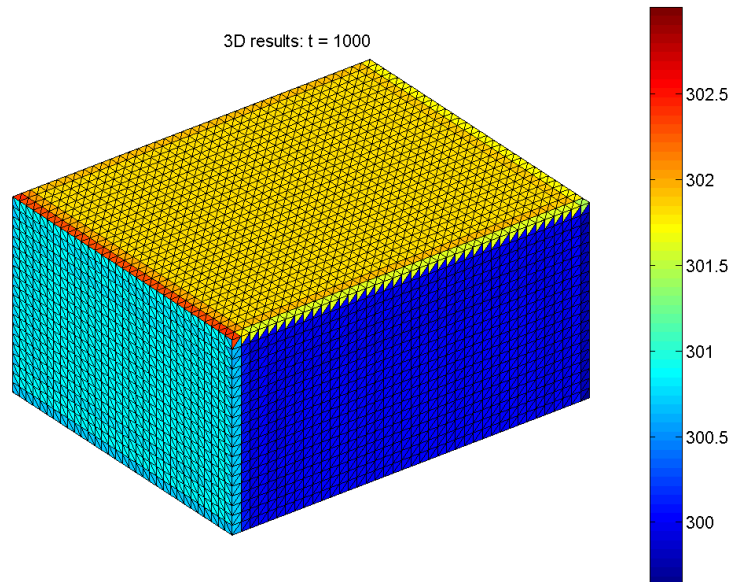


Figure A6: Temperature distribution on a 100 mm-thick block surface (3D results)

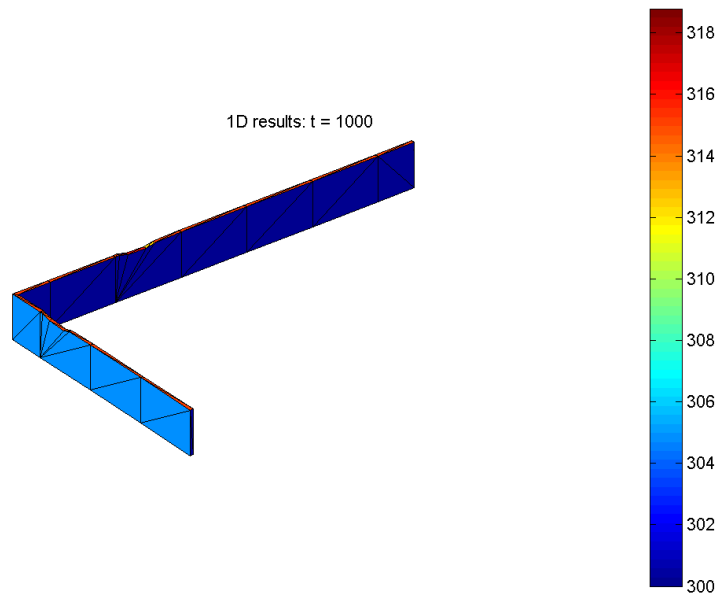


Figure A7: Temperature distribution on Wall2 (1D results)

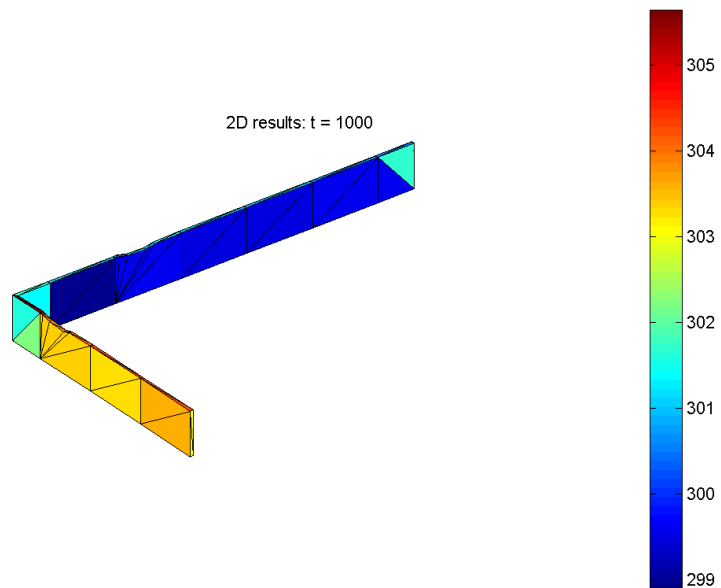


Figure A8: Temperature distribution on Wall2 (2D results)

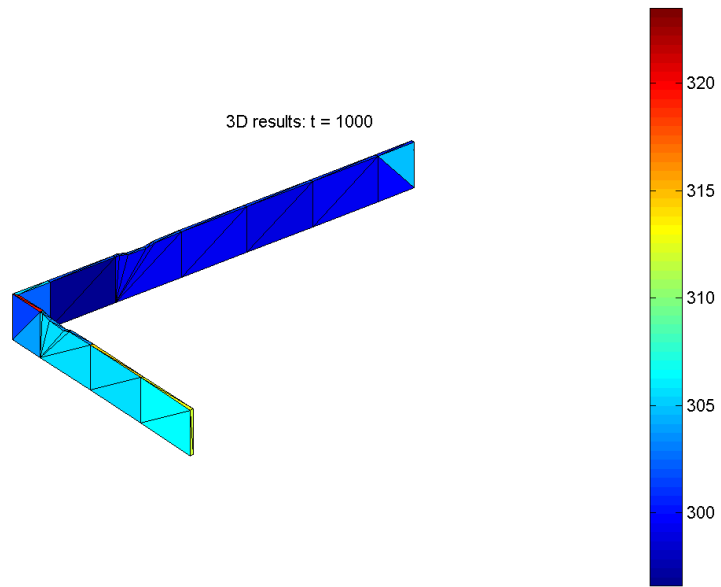


Figure A9: Temperature distribution on Wall2 (3D results)

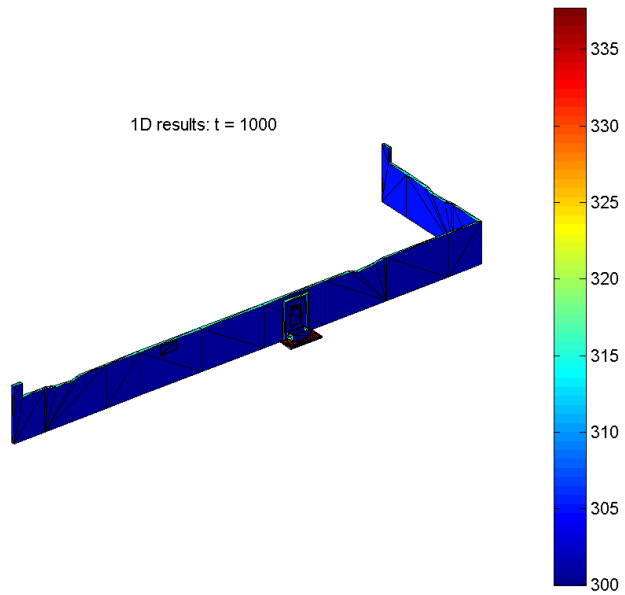


Figure A10: Temperature distribution on Wall3 (1D results)

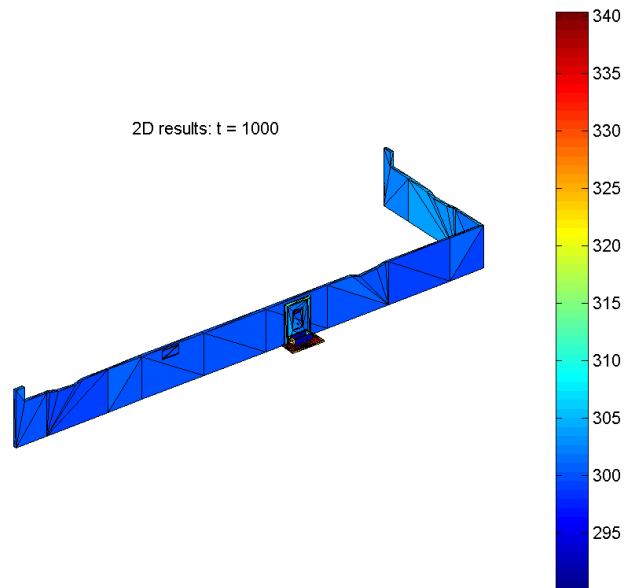


Figure A11: Temperature distribution on Wall3 (2D results)

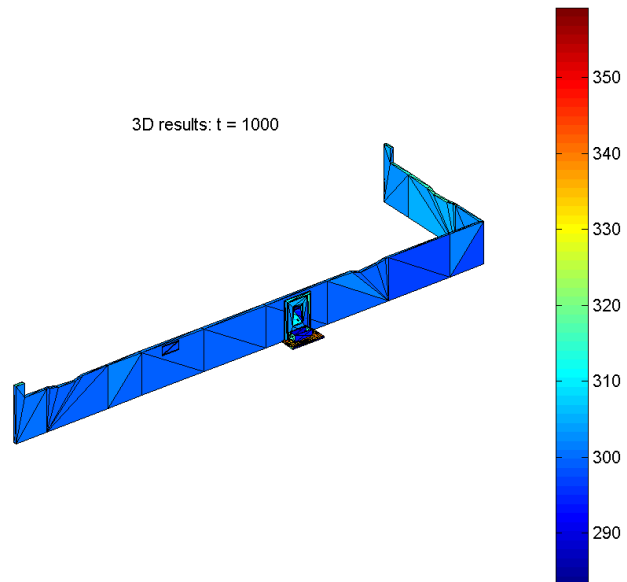


Figure A12: Temperature distribution on Wall3 (3D results)

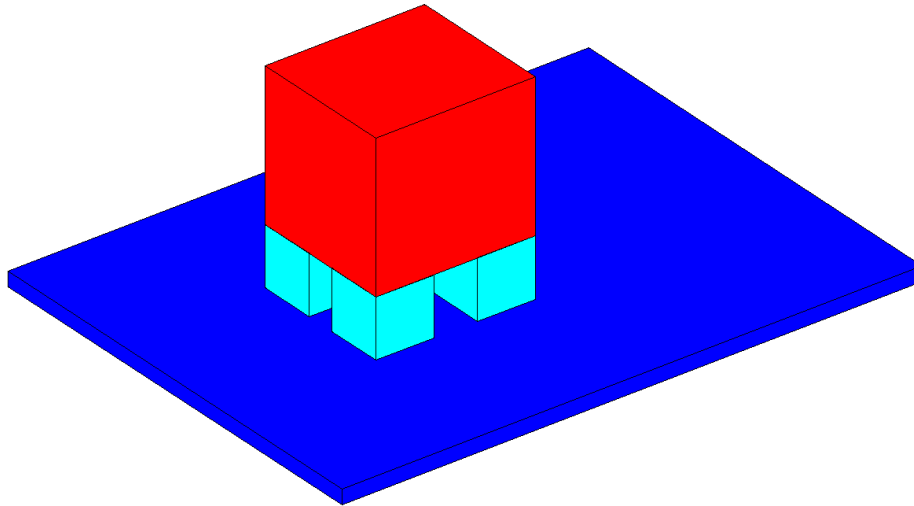


Figure A13: Engine block model

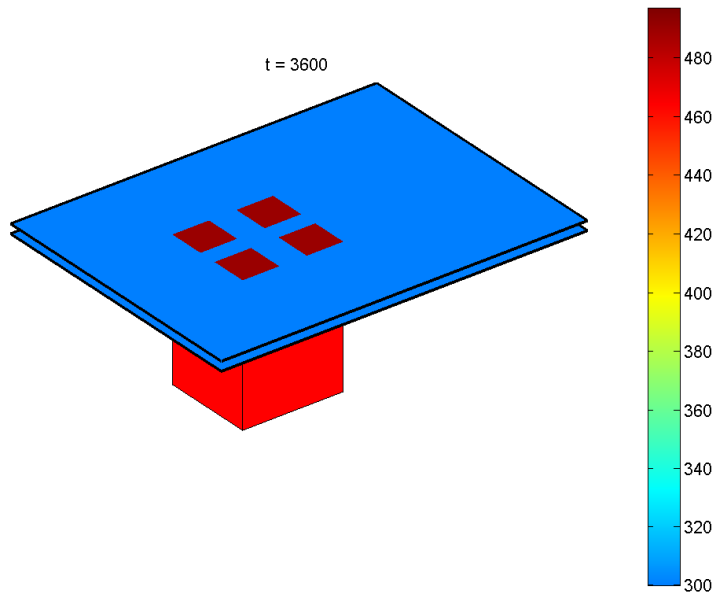


Figure A14: Temperature distribution near engine block (1D results)

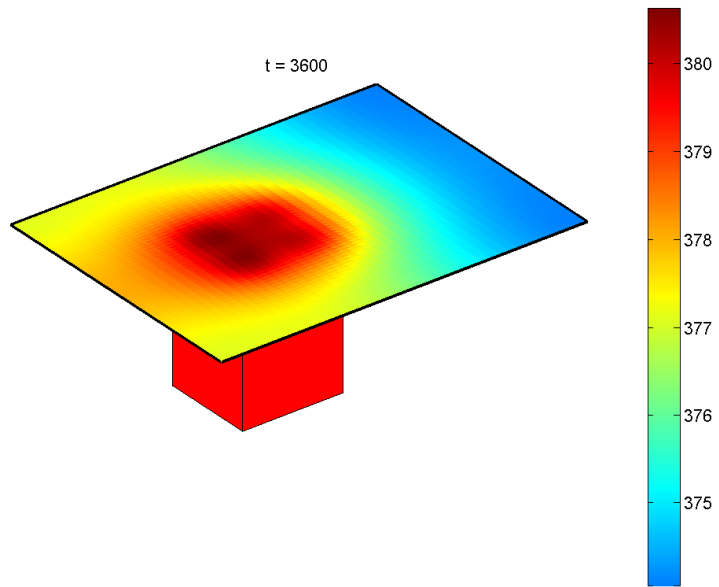


Figure A15: Temperature distribution near engine block (2D results)

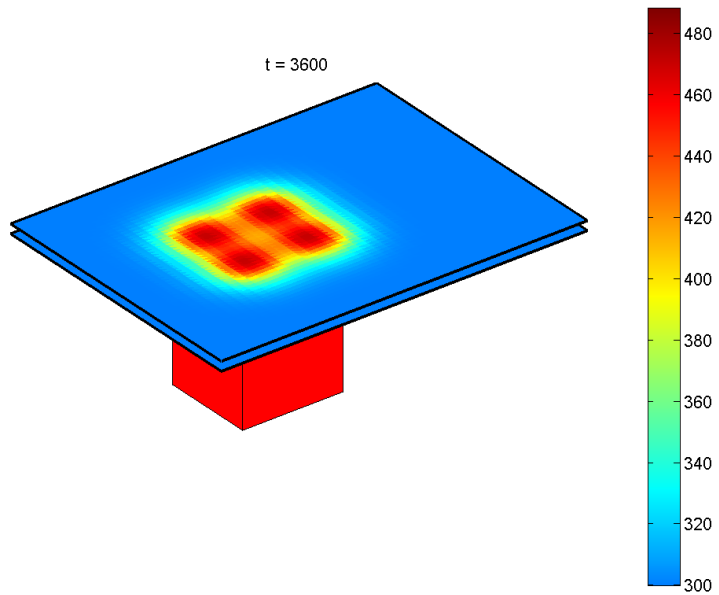


Figure A16: Temperature distribution near engine block (3D results)

UNCLASSIFIED

<b>DEFENCE SCIENCE AND TECHNOLOGY GROUP DOCUMENT CONTROL DATA</b>			1. DLM/CAVEAT (OF DOCUMENT)	
2. TITLE Finite Element Modelling of Heat Exchange with Thermal Radiation		3. SECURITY CLASSIFICATION (FOR UNCLASSIFIED REPORTS THAT ARE LIMITED RELEASE USE (L) NEXT TO DOCUMENT CLASSIFICATION)  Document (U) Title (U) Abstract (U)		
4. AUTHOR Leonid K Antanovskii		5. CORPORATE AUTHOR Defence Science and Technology Group PO Box 1500 Edinburgh, South Australia 5111, Australia		
6a. DST Group NUMBER DST-Group-TR-3345	6b. AR NUMBER 016-809	6c. TYPE OF REPORT Technical Report	7. DOCUMENT DATE February, 2017	
8. Objective ID AV12597362	9. TASK NUMBER AIR07/213	10. TASK SPONSOR RAAF Air Combat Group		
13. DST Group Publications Repository <a href="http://dspace.dsto.defence.gov.au/dspace/">http://dspace.dsto.defence.gov.au/dspace/</a>		14. RELEASE AUTHORITY Chief, Weapons and Combat Systems Division		
15. SECONDARY RELEASE STATEMENT OF THIS DOCUMENT  <i>Approved for public release</i>  OVERSEAS ENQUIRIES OUTSIDE STATED LIMITATIONS SHOULD BE REFERRED THROUGH DOCUMENT EXCHANGE, PO BOX 1500, EDINBURGH, SOUTH AUSTRALIA 5111				
16. DELIBERATE ANNOUNCEMENT				
17. CITATION IN OTHER DOCUMENTS No Limitations				
18. RESEARCH LIBRARY THESAURUS Science, Mathematics, Finite Element Method, Thermal Radiation				
19. ABSTRACT  This report addresses the mathematical and numerical modelling of heat exchange in a solid object with the effect of thermal radiation included. Three models are analysed, the general three dimensional model and two approximate models. Based on Finite Element Method (FEM), a fully vectorized MATLAB <sup>®</sup> solver is developed for the three models, and simulation results are compared. The developed code can be used to enhance the VIRSuite software developed in DST Group for simulation of weapon-target engagement.				

UNCLASSIFIED